Energy Proceedings
Vol 31, 2023
ISSN 2004-2965

MgO induced $LiNO_3$/NaCl molten salt nanocomposite with synergetic enhancement in C_p and solidus thermal conductivity

Qingyang Luo [1], Xianglei Liu [1, 2*]

1 School of Energy and Power Engineering, Nanjing University of Aeronautics and Astronautics, Nanjing 210016

2 Integrated Energy Institute, Nanjing University of Aeronautics and Astronautics, Nanjing, 210016 (*Corresponding Author)

ABSTRACT

Insight into the development of the next generation concentrated solar power plant (CSP), molten salts are the most promising candidate in storing the thermal energy, although it still suffers from low energy storage density and thermal conductivity. Recently, various nano-additives were verified to have the potential in promoting the thermal properties of molten salts. In this work, 50nm MgO nanoparticles with a mass fraction of 1% to 10% are dispersed into the $LiNO_3$/NaCl eutectic, and the thermal properties consisting of thermal conductivity, specific heat capacity (C_p), phase change enthalpy, and viscosity are evaluated by experiments. Compared with many other ceramic nanoparticles, only the MgO dispersed nanomaterial obtains both enhancement in solidus thermal conductivity and C_p, which are improved up to 63.5% and 28% at 4wt.% MgO, respectively. On the contrary, the phase change enthalpy and viscosity are developed toward the negative direction, but within the acceptable limit. Combining the above results, molten salts with nanoparticles added are still desirable candidates to meet the demand of the next generation CSP.

Keywords: concentrated solar power, molten salt, thermal properties, thermal energy storage

NONMENCLATURE

Abbreviations	
CSP	Concentrated solar power
DSC	Differential scanning calorimeter
MD	Molecular dynamics
PCM	Phase change material
PDOS	Phonon density of state
SEM	Scanning electron microscopy
TES	Thermal energy storage
Symbols	
C_p	Specific heat capacity ($J \cdot g^{-1} \cdot °C^{-1}$)
H	Phase change enthalpy ($J \cdot g^{-1}$)
R_b	Interfacial thermal resistance ($K \cdot m^2/W$)
λ	Thermal conductivity ($W \cdot m^{-1} \cdot K^{-1}$)
η	Viscosity (cp)

1. INTRODUCTION

Solar energy, the primitive energy source on the earth, has been attracting more and more global attention, due to serious climate change and fossil energy depletion. Since the photovoltaic power generation still suffers low incident photon-to-electron conversion efficiency (IPCE) and solar source intermittence problems, concentrated solar power plants (CSP) with thermal energy storage (TES) systems are widely investigated recently. Fig. 1. shows a classical CSP with a TES system [1]. In this way, the solar energy can be stored as heat and provide an output power more stable, which then significantly improves the efficiency in solar energy utilization. TES materials are one of the most important parts of CSP because they determine the energy storage density of the system. Phase change materials (PCMs) are desirable candidates for the TES system, due to their extremely high latent heat with nearly unchanged temperature during phase change. However, conventional PCMs usually possess a very low thermal conductivity, which will damage the output power. And with the development of global society, energy demand is growing exponentially. As a

result, it is an urgent mission to develop PCMs with high thermal conductivity and energy storage density.

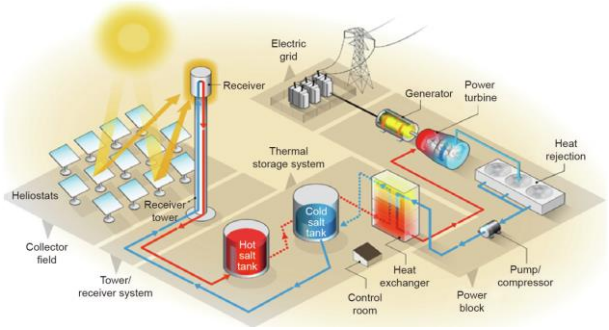

Fig. 1. A state-of-art CSP with molten salt TES system [1]

Researchers found that it is a simple strategy to enhance the overall thermal conductivity of PCMs by embedding porous scaffolds with high bulk thermal conductivity. Yu et. al. [2] have successfully fabricated a graphene foam-CNT hybrid structure, and made a composite with polyethylene glycols (PEG). The results show that the composite exhibited a thermal conductivity enhancement up to 118%, compared with pure PCM. But the PCM loading was less than 80 wt.%, which would deteriorate the energy storage density. For molten salt based PCMs, the scaffold should also be able to stand at a high temperature with corrosion resistance. So, ceramics later came into the eye of researchers. Our previous works [3-5] successfully fabricated AlN and SiC based molten salt composites, and the thermal conductivity of these composites is also greatly promoted. But the energy storage density is still precluded. Nevertheless, other ultralight foams [6] are too cumbersome and expensive in synthesis.

Moreover, nanoparticles (such as SiO_2, Al_2O_3, etc.) dispersed molten salt composites (called nanofluid) are found to have enhanced liquidus thermal conductivity and specific heat capacity (C_p). Although the thermal conductivity enhancing percentage is not as high as highly conductive scaffolds, the energy storage density is guaranteed. Yasinskiy et. al. [7] argued that the thermal conductivity is improved by 25.8%, when TiO_2 nanoparticles are added in the experiment. Li [8] and Yu [9] et. al. proved the nanoparticle induced thermal conductivity enhancement by molecular dynamics (MD) simulation, and the mechanism is also delivered. The increment in thermal conductivity may be attributed to 1), the intrinsically high thermal conductivity of nanoparticles compared to PCMs, 2) the introduction of nanoparticles can improve the probability and frequency of collision, further enhancing the Brownian motion and micro-convection of the nanofluid. However, the solidus thermal conductivity of nanoparticle dispersed molten salt is not mentioned in the corresponding research. Especially for middle and high temperature PCMs, the solidus thermal conductivity exactly plays an important role that will influence the heat transfer. But according to our previous work [10], the solidus thermal conductivity of 1 wt.% 50nm SiO_2 dispersed $LiNO_3$/NaCl molten salt is just 60% as that of the pure eutectic, and the reason is unfolded by MD simulations. In detail, we found that the interfacial thermal resistance (R_b) is very high up to 1.825×10^{-7} K·m^2/W between SiO_2 and $LiNO_3$, and too many interfaces are introduced into the PCMs, which results in severe phonon scattering. Nevertheless, the Brownian motion and micro-convection are suppressed at solid state as well. Consequently, it's no easy task to improve the thermal conductivity at all temperature ranges.

As for the C_p increment, the mechanism has been revealed by other researchers in the last few years. Qiao et. al. [11] proposed SiO_2-KNO_3 nanofluid, and claimed that the C_p is enhanced impressively, and it contradicts the results calculated with the equilibrium theory of C_p. Hu et. al. [12] carried out a study on Al_2O_3-Solar salt (60wt.% $NaNO_3$-40wt.% KNO_3). The experiment and MD simulation results both proved the enhancement in C_p. And they suggested that the Coulombic interaction between the nanoparticle and base salt may cause the C_p to increase. Svobodova-Sedlackova et. al. [13] concluded that the reasons for the C_p increment of nanofluid is attributed to 1) the high surface energy between nanoparticle and eutectic, 2) interfacial thermal resistance at the interface, 3) the semi-solid layer around the nanoparticle. Moreover, Rizvi et. al. [14] further found the dendritic structure formed by eutectic which can enhance the C_p. But the heat of fusion will receive an abnormal decrease, because the dendritic structure will not melt at the melting point.

In this paper, $LiNO_3$/NaCl (92.5:7.5 in molar ratio) eutectic is chosen as the base salt, due to its high phase change enthalpy (~350 J·g^{-1}) and middle temperature melting point (~225°C). Subsequentially, nanomaterials with 1-10 wt.% 50nm MgO nanoparticle added are fabricated. The thermal conductivity and C_p are measured to have great improvements of up to 63.4% and 28%, respectively. And the viscosity of eutectic and 4 wt.% MgO nanomaterial are tested. Although the viscosity of 4 wt.% MgO nanomaterial gets higher, only a 15% increment is detected at 360°C, compared to the pure eutectic. So, the fluidity of nanomaterial may not be affected much by 50nm MgO nanoparticles.

2. EXPERIMENT

2.1 Materials

SiO_2, CuO, SiC, TiN, TiO_2, and MgO nanoparticles (~50 nm, 99.9% metal basis) are purchased from Shanghai Macklin Biochemical Co., Ltd., China. $LiNO_3$ with a purity of 99.9% is obtained from Shanghai Aladdin BioChem Technology Co., Ltd., China. And NaCl is bought from Nanjing Chemical Reagent Co., Ltd., China.

2.2 Synthesis of nanomaterial

Initially, $LiNO_3$ and NaCl with a molar ratio of 92.5-7.5 is weighed on an analytical balance (CPA225D, Sartorius, Germany). and then 1-10wt.% MgO nanoparticle is added into the salt mixture. After that, the mixture powder is dissolved in deionized water and sonicated for 2 hours in the ultra-sonicator (Scientz-CHF-5B, Ningbo Scientz Biotechnology Co. Ltd., China) to obtain a good dispersion of nanoparticles. Later, the solution is pulled into a glass petri dish, and placed on a hot plate at 150°C until it is fully dried. Finally, the sample is put into a drying cabinet and ground to fine powder in an agate mortar.

2.3 Characterization

The thermal conductivity of different samples is measured by the laser flash method (LFA 500, Linseis, Germany). The mixed powder is first pressed into a tablet under 18 MPa to form a cylinder with a diameter of 12.7mm and a height of around 2mm. And the tablet is then loaded into the specialized graphite crucible for further test. A laser pulse with fixed power is shot to heat the bottom of the tablet, and then the temperature rise at the top is measured by the instrument over time to calculate the thermal diffusivity. All the samples are tested 5 times to ensure reliable data. The thermal conductivity calculated from thermal diffusivity is shown below:

$$\lambda=\alpha \cdot \rho \cdot C_p \quad (1)$$

where, λ is the thermal conductivity ($W \cdot m^{-1} \cdot K^{-1}$), α is the thermal diffusivity ($mm^2 \cdot s^{-1}$), ρ is the density ($g \cdot cm^{-3}$), and the C_p ($J \cdot g^{-1} \cdot °C^{-1}$) and the phase change enthalpy are measured by a differential scanning calorimeter (DSC 25, TA Instrument, USA). The mixed power with 10-15 mg is sealed in an aluminum hermetic crucible and then heated from 0°C to 350°C with a ramping rate of 2°C/min. The experiments of all samples are conducted for at least 2 cycles to eliminate the moisture under N_2 flow, and the heat flow curves are monitored by the differential scanning calorimetry technique. The C_p of samples is obtained by comparing the heat flow data with the standard sapphire, which is expressed by Eq. (2). And the phase change enthalpy is integrated from the peak of the heat flow curve.

$$C_{p,\text{sample}} = \frac{q_{\text{sample}} - q_{\text{baseline}}}{q_{\text{sapphire}} - q_{\text{baseline}}} \cdot \frac{m_{\text{sapphire}}}{m_{\text{sample}}} \cdot C_{p,\text{sapphire}} \quad (2)$$

where, q is the heat flow ($mW \cdot mg^{-1}$), m is the mass (mg) of samples.

The viscosity of the fluid is measured by a rotary viscometer in the temperature range from 250°C to 500°C. The measurement is mainly carried out in the air with a fixed low rotational speed of 30 rpm to form a stable laminar flow. In detail, 80g mixed powder is first filled in a cylindrical nickel crucible (to resist corrosion), and then melted in the vertically assembled tube furnace, which is served as the heater of the rotary viscometer. After the sample is completely melted, a nickel spindle is then immersed into the fluid, which connects with the torquemeter (DV2TLVTJ0, Ametek Brookfield, USA) by a nickel wire. Prior to the viscosity measurement of the fluids, the viscometer is first calibrated with deionized water at 5°C. And the measured value of water is around 0.8 cp, which shows the reliability of the rotary viscometer. Both of the molten salts with 4wt.% MgO nanoparticle and $LiNO_3$/NaCl are tested from 240°C to 420°C with a temperature interval of around 20°C. Before the viscosity measurement, the samples are thermostat at the target temperature for 30min to ensure the testing accuracy.

3. RESULTS AND DISCUSSION

3.1 Morphology

In general, the C_p of material is closely related to its phase and interface. Therefore, to reveal the microstructure of eutectic and nanomaterials, Scanning Electron Microscopy (SEM, GeminiSEM 300, ZEISS, Germany) is employed to capture the morphology of prepared materials. And SEM images of eutectic, 4wt.% and 10wt.% nanomaterials are plotted in Fig. 2. As shown in Fig. 2a, the grains of eutectic are very complete and clear, and the surface of eutectic is smooth. With the dispersing of MgO nanoparticles, little spots and holes appear on the surface of the eutectic, surrounding the nanoparticles (Fig. 2b). With the increase of MgO nanoparticles mass fraction, take 10wt.% MgO nanomaterial as an example (Fig. 2c), the crystal surface becomes rough and the nanoparticles appear serious agglomeration. As a result, more mass fraction of MgO nanoparticles is not always better. On

the one hand, the agglomeration of nanoparticles, which is inevitable at present, has no help in enhancing the C_p. On the other hand, the addition of a large number of nanoparticles forms too many interfaces, which will seriously increase the phonon-phonon scattering rate, further damaging the thermal conductivity of nanomaterials.

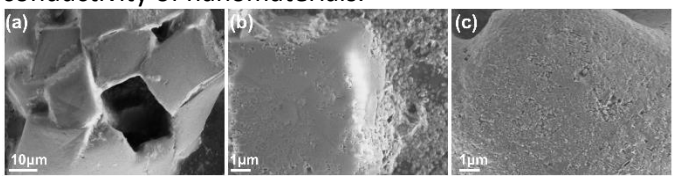

Fig. 2. SEM images of (a) eutectic, (b) 4wt.% and (c) 10wt.% nanomaterials

3.2 Solidus thermal conductivity

Thermal conductivity is an important property for TES materials. A material with a higher thermal conductivity can store/release the thermal energy faster, so as to decrease the heat dissipation to the environment, which can greatly improve efficiency. Since the enhanced liquidus thermal conductivity of the nanofluid is investigated by others sufficiently, the solidus thermal conductivity, which is also a vital property for middle and high temperature TES materials, is the main concern of this section. Therefore, to enhance the solidus thermal conductivity of the eutectic, 6 kinds of nanoparticles including SiO_2, CuO, SiC, TiN, TiO_2, and MgO are dispersed into the eutectic with 1wt.%, respectively. And the thermal conductivity of these tablets is measured by the laser flash method. Fig. 3 exhibits the thermal conductivity of different samples. It is clear that the thermal conductivity of SiO_2, CuO, SiC, TiN, TiO_2 dispersed nanomaterials are all lower than the pure eutectic, at room temperature. Nevertheless, only the 50nm MgO dispersed nanomaterial demonstrates the potential of high thermal conductivity. In that case, nanomaterials with 1, 2, 3, 4, 5, 7.5, 10 wt.% (abbreviated as X-MS, which means X wt.% MgO dispersed molten salt) are prepared and tested. The thermal conductivity versus mass fraction is first increased and then decreased, and the maximum value of 1.625 $W \cdot m^{-1} \cdot K^{-1}$ is received at MgO mass fraction of 4%, which is 63.5% higher than that of the pure eutectic (0.994 $W \cdot m^{-1} \cdot K^{-1}$). The main reason may be attributed to the low interfacial thermal resistance between MgO and eutectic. So, the thermal conductivity is enhanced at first. However, with the increase of MgO mass fraction, the concentration of interface is increased, and then the phonon scattering at the interface becomes a key factor that will deteriorate the thermal conductivity.

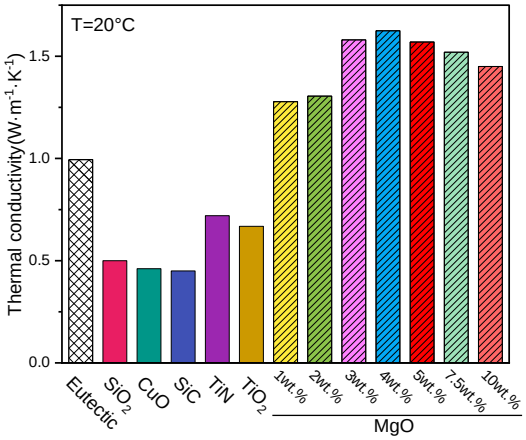

Fig. 3. The thermal conductivity of pure eutectic and nanomaterials with different kinds of nanoparticles. For MgO dispersed nanomaterials, different mass fraction is also tested.

To verify the interfacial effect on the solidus thermal conductivity, the interfacial thermal resistance and the phonon density of state (PDOS) are calculated by MD simulations at 300K, as described in our previous study [10]. The R_b between MgO and the eutectic is calculated as 2.637×10^{-9} $K \cdot m^2/W$, which is impressively lower than that between SiO_2 and $LiNO_3$ (R_b=1.825×10^{-7} $K \cdot m^2/W$ [10]). And the PDOS of MgO and the eutectic is plotted in Fig. 4, compared to the PDOS of SiO_2 and $LiNO_3$ (in the inset of Fig. 4), the PDOS of the eutectic is very similar to the $LiNO_3$, which is mainly due to the low molar ratio of NaCl. However, the PDOS of MgO is different from that of SiO_2. The phonon vibration of MgO mainly lies in a lower frequency, this is the main reason why the R_b is lower than other conventional nanoparticle-salt pairs. Qiu et. al. [15] systematically studied the factor that affects interfacial thermal transport. And they claimed that the low-frequency phonon is more helpful in the thermal transport at the interface. And this is consistent with our computational and experimental results.

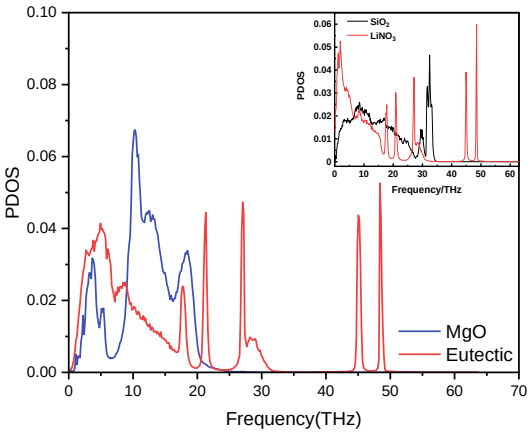

Fig. 4. The comparison of phonon density of state (PDOS) between MgO and the eutectic, inset demonstrated the PDOS of SiO_2 and $LiNO_3$, which is reported in [10]

3.3 Specific heat capacity

Now that the thermal conductivity of MgO dispersed nanomaterials is proved to have a positive performance. For the pursuit of high energy storage density, the C_p is measured by DSC as well, which is shown in Fig. 5. The C_p of 1 and 2-MS is lower than that of the eutectic, due to the low interfacial thermal resistance. Starting at 3wt.% MgO, the C_p becomes higher than the eutectic. And the maximum C_p also appears at 4wt.%, which is 28% higher than that of the eutectic at 100°C and 12.4% at 300°C. When the mass fraction exceeds 4%, nanoparticles will face serious agglomeration, as a result, the contribution of interfacial effect on C_p is weakened. The above results represent that there is the best mass fraction of MgO nanoparticle which can maximize the enhancement in thermal conductivity and C_p of the eutectic. And the best mass fraction is highly related to the interfacial effect and the degree of agglomeration.

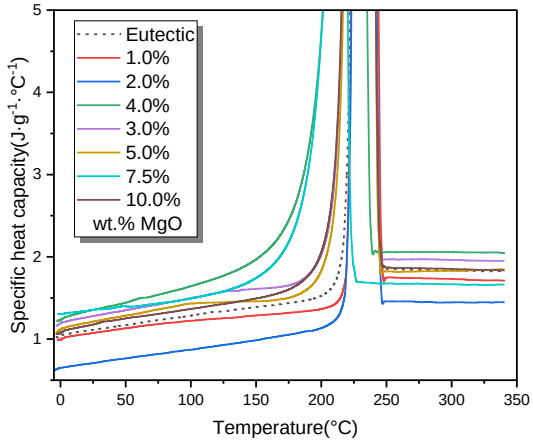

Fig. 5. The specific heat capacity of MgO dispersed nanomaterials with different mass fraction from 0-350°C.

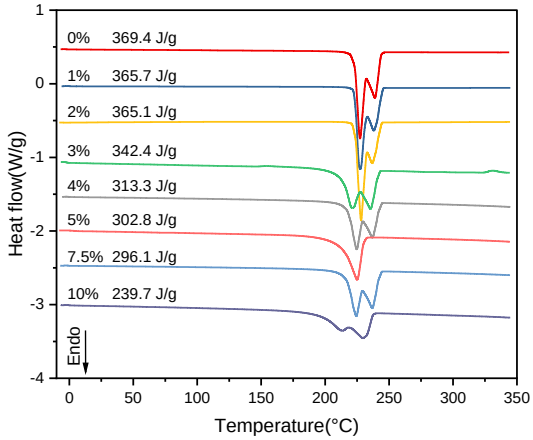

Fig. 6. The heat flow curve and the phase change enthalpy during melting of samples with different mass fraction of 50nm MgO nanoparticle.

The heat flow curves of samples with different mass fractions of 50nm MgO nanoparticles are plotted in Fig. 6 to analyze the change in melting point and phase change enthalpy. It is clear that no significant alter is found for melting point (220°C). The enthalpy of eutectic is measured as 369.4 $J \cdot g^{-1}$. And the enthalpy is decreased with the increase of MgO mass fraction, naturally. A sharp decrease is also detected for samples with improved C_p, indicating a large number of dendritic structures are formed. As a result, the nanoparticles are not supposed to be added too much in the eutectic.

3.4 Viscosity

The synergetic increase in thermal conductivity and C_p has been realized by MgO nanoparticles. But the viscosity should also be investigated, since it affects the convective heat transfer during phase change. A PCM with relatively high viscosity may have a low convective heat transfer rate during melting, considering the natural convection. Nevertheless, adding nanoparticles in the molten salt will inevitably increase the viscosity, which is proved by many pieces of literature [16-18]. So, the viscosity of eutectic and 4-MS is measured by a rotary viscometer at the temperature ranging from 240°C to 420°C. As Fig. 7 depicts, the viscosity of eutectic and 4-MS both decreases with the increase of temperature. With the existence of MgO nanoparticles, the viscosity of 4-MS is higher than that of eutectic. However, the increment is relatively low, where the enhancement of 24.7% and 15% is appeared at 250°C and 360°C, respectively. And as the temperature rises the difference in viscosity gradually decreases.

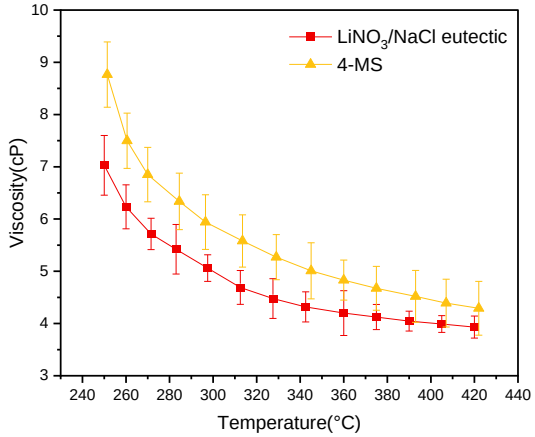

Fig. 7. The viscosity of $LiNO_3$/NaCl eutectic and nanomaterial at 4 wt.% MgO nanoparticles.

4. CONCLUSION

This work proposes 50nm MgO dispersed $LiNO_3$/NaCl nanomaterials to store the thermal energy, hoping to meet the demand of next generation CSP. Subsequentially, 1-10wt.% MgO dispersed $LiNO_3$/NaCl nanomaterials are fabricated and the thermal

properties are tested. Among different nanoparticles, only MgO dispersed nanomaterials grasp both the solidus thermal conductivity and C_p increment (64.3% and 28%, respectively) when dispersed in $LiNO_3$/NaCl eutectic. And the best mass fraction of MgO nanoparticle is around 4wt.%, which is different from conventional cases. The reason is attributed to the low interfacial thermal resistance between the eutectic and MgO. Furthermore, adding nanoparticles will naturally deteriorate the phase change enthalpy during the melting and viscosity of proposed nanomaterials. But the negative effect is acceptable. Therefore, with the desired thermal conductivity and C_p, the MgO dispersed nanomaterials have the potential in the TES application of next generation CSP.

ACKNOWLEDGEMENT

This work is mainly supported by National Key R&D Program of China (No. 2018YFA0702300), And National Natural Science Foundation of China (No. 51820105010 and 52076106).

REFERENCE

[1] Ding W, Bauer T. Progress in Research and Development of Molten Chloride Salt Technology for Next Generation Concentrated Solar Power Plants. Engineering. 2021;7:334-47.

[2] Yu Z, Feng D, Feng Y, Zhang X. Thermal conductivity and energy storage capacity enhancement and bottleneck of shape-stabilized phase change composites with graphene foam and carbon nanotubes. Compos Pt A-Appl Sci Manuf. 2022;152:106703.

[3] Xu Q, Liu X, Luo Q, Song Y, Wang H, Chen M, et al. Bifunctional biomorphic SiC ceramics embedded molten salts for ultrafast thermal and solar energy storage. Mater Today Energy. 2021;21:100764.

[4] Liu XL, Wang HL, Xu Q, Luo QY, Song YA, Tian Y, et al. High thermal conductivity and high energy density compatible latent heat thermal energy storage enabled by porous AlN ceramics composites. Int J Heat Mass Transf. 2021;175:121405.

[5] Liu X, Song Y, Xu Q, Luo Q, Tian Y, Dang C, et al. Nacre-like ceramics-based phase change composites for concurrent efficient solar-to-thermal conversion and rapid energy storage. Sol Energy Mater Sol Cells. 2021;230:111240.

[6] Vu MC, Thieu NAT, Choi WK, Islam MA, Kim S-R. Ultralight covalently interconnected silicon carbide aerofoam for high performance thermally conductive epoxy composites. Compos Pt A-Appl Sci Manuf. 2020;138:106028.

[7] Yasinskiy A, Navas J, Aguilar T, Alcántara R, Gallardo JJ, Sánchez-Coronilla A, et al. Dramatically enhanced thermal properties for TiO2-based nanofluids for being used as heat transfer fluids in concentrating solar power plants. Renew Energy. 2018;119:809-19.

[8] Li Z, Cui L, Li B, Du X. Enhanced heat conduction in molten salt containing nanoparticles: Insights from molecular dynamics. Int J Heat Mass Transf. 2020;153:119578.

[9] Yu Y, Tao Y, He Y-L. Molecular dynamics simulation of thermophysical properties of NaCl-SiO2 based molten salt composite phase change materials. Appl Therm Eng. 2020;166:114628.

[10] Luo Q, Liu X, Wang H, Xu Q, Tian Y, Liang T, et al. Synergetic enhancement of heat storage density and heat transport ability of phase change materials inlaid in 3D hierarchical ceramics. Appl Energy. 2022;306:117995.

[11] Qiao G, Lasfargues M, Alexiadis A, Ding Y. Simulation and experimental study of the specific heat capacity of molten salt based nanofluids. Appl Therm Eng. 2017;111:1517-22.

[12] Hu Y, He Y, Zhang Z, Wen D. Effect of Al 2 O 3 nanoparticle dispersion on the specific heat capacity of a eutectic binary nitrate salt for solar power applications. Energy Conv Manag. 2017;142:366-73.

[13] Svobodova-Sedlackova A, Barreneche C, Alonso G, Fernandez AI, Gamallo P. Effect of nanoparticles in molten salts – MD simulations and experimental study. Renew Energy. 2020;152:208-16.

[14] Rizvi SMM, Shin D. Mechanism of heat capacity enhancement in molten salt nanofluids. Int J Heat Mass Transf. 2020;161:120260.

[15] Qiu L, Zhang X, Guo Z, Li Q. Interfacial heat transport in nano-carbon assemblies. Carbon. 2021;178:391-412.

[16] Far BE, Rizvi SMM, Nayfeh Y, Shin D. Investigation of heat capacity and viscosity enhancements of binary carbonate salt mixture with SiO2 nanoparticles. Int J Heat Mass Transf. 2020;156:119789.

[17] El Far B, Rizvi SMM, Nayfeh Y, Shin D. Study of viscosity and heat capacity characteristics of molten salt nanofluids for thermal energy storage. Sol Energy Mater Sol Cells. 2020;210:110503.

[18] Nithiyanantham U, González-Fernández L, Grosu Y, Zaki A, Igartua JM, Faik A. Shape effect of Al2O3 nanoparticles on the thermophysical properties and viscosity of molten salt nanofluids for TES application at CSP plants. Appl Therm Eng. 2020;169:114942.